



Contents lists available at ScienceDirect

Earth and Planetary Science Letters

journal homepage: www.elsevier.com/locate/epsl

Experimental evidence for rapid water exchange between melt inclusions in olivine and host magma

Maxim Portnyagin^{a,b,*}, Renat Almeev^c, Sergei Matveev^d, François Holtz^c

^a Division of the Ocean Floor, IFM-Geomar, Wischhofstr. 1-3, 24148 Kiel, Germany

^b Vernadsky Institute, Kosigin st. 19, 119991, Moscow, Russia

^c University of Hannover, Institute of Mineralogy, Callinstr. 3, Hannover, 30167, Germany

^d University of Alberta, Department of Earth and Atmospheric Sciences, 1-26 Earth Sciences Building, Edmonton, Alberta, Canada T6G 2E3

ARTICLE INFO

Article history:

Received 23 November 2007

Received in revised form 7 May 2008

Accepted 15 May 2008

Available online 28 May 2008

Editor: C.P. Jaupart

Keywords:

olivine

melt inclusion

water

re-equilibration

experiment

ABSTRACT

Melt inclusions in olivine are source of unique information about primitive mantle melts. Here we report results of an experimental study aimed at evaluating the ability of olivine to isolate chemically melt inclusions from the host magma after their entrapment. We demonstrate that nearly 'dry' melt inclusions from Galapagos Plateau basalt can gain up to 2.5 wt.% of water if they are placed for 2 days in a water-bearing melt at 200 MPa and 1140 °C. The major element composition of melt inclusions also changed significantly, as a result of a re-equilibration with the olivine host mineral, whereas no significant changes were detected for incompatible trace elements. Our results indicate that inclusions in olivine can rapidly and selectively exchange water with the matrix melt, probably, through combination of proton diffusion and molecular water transport along dislocations in olivine. The fast water transport explains element fractionation, which is not predictable from the theory of magmatic processes. An efficient re-equilibration of melt inclusions with matrix melt can explain the decoupling of water and incompatible trace elements (e.g., H₂O vs. K₂O) reported for suites of primitive inclusions from mid-ocean-ridge setting and island arcs. Rare cases of well preservation of initial water content in suites of co-genetic inclusions imply very short residence time (a few hours) of the olivine phenocrysts in magma with contrasting water content during fractionation and transport to the surface and rapid quenching upon eruption.

© 2008 Elsevier B.V. All rights reserved.

1. Introduction

A considerable knowledge about Earth magmatism and, particularly, about the distribution and abundance of volatiles (H₂O, CO₂, S, halogens) in the mantle comes from the studies of melt inclusions in minerals. These microscopic droplets of melt, usually occurring as glass (± crystals) at room temperature, are occasionally captured by growing crystals at depth (e.g. Roedder, 1984). Melt inclusions in olivine are of particular interest, since olivine is the first silicate mineral crystallizing from mantle-derived magmas on their pathway to the surface. This mineral is thus a potential host for very primitive mantle melts (Sobolev and Shimizu, 1993; Schiano, 2003). A common premise of melt inclusion studies is that olivine can preserve the chemical composition of melt inclusions, at least, with respect of many trace elements and volatiles (Sobolev, 1996; Danyushevsky et al., 2002a). Several studies, however, demonstrated that olivine is not an ideal container for melt inclusions. Melt inclusions can change composition on short time scale (days to a few years) due to diffusive Fe–Mg re-equilibration with olivine and with

matrix melt (Danyushevsky et al., 2000; Gaetani and Watson, 2000). Diffusive hydrogen and, possibly, hydroxyl loss were shown to be a common and rapid process during 1 atm homogenization experiments with hydrous melt inclusions and possibly during slow cooling in nature (Sobolev et al., 1989; Danyushevsky et al., 2002a; Hauri, 2002; Massare et al., 2002; Wallace, 2005). Diffusion coefficients for many incompatible trace elements (e.g., REE) in olivine were shown to be sufficiently high to allow diffusive re-equilibration of melt inclusions on the time scale of tens to hundreds years (Spandler et al., 2007).

Despite the significant progress achieved in the past years in our understanding of the origin and evolution of melt inclusions, there are only few available experimental data allowing us to evaluate quantitatively the re-equilibration processes of melt inclusions for major, volatile and trace elements as a function of time. This experimental study is aimed to test the ability of olivine to isolate chemically melt inclusions from the host magma after their entrapment, with particular emphasis on the behavior of water. We demonstrate that nearly 'dry' melt inclusions can gain up to 2.5 wt.% of water if they are placed for 2 days in a water-bearing melt. Our results have several implications for the interpretation of melt inclusion data and indicate that a preservation of initial water content is only possible when residence time of olivine phenocrysts in magma with contrasting water content is in the order of a few hours.

* Corresponding author. Division of the Ocean Floor, IFM-Geomar, Wischhofstr. 1-3, 24148 Kiel, Germany.

E-mail address: mportnyagin@ifm-geomar.de (M. Portnyagin).

2. Methods

2.1. Starting materials

Natural olivines containing melt inclusions (Fig. 1a) were separated from an olivine-plagioclase-pyroxene-bearing phyric submarine th-

leitic basalt from the Galapagos Plateau (sample PL02-24-33 provided by D. Christie). Olivine phenocrysts in the sample are up to 1.5 mm in size and have homogeneous cores ranging from Fo₇₉ to Fo_{88.5} (Fig. 2). The olivines are surrounded by ~50 μm-wide normally zoned rim, where olivine composition changes gradually to Fo₇₉₋₈₁. Similarly low-Fo olivines also occur as microliths in the groundmass glass (Fig. 2). The Fe-

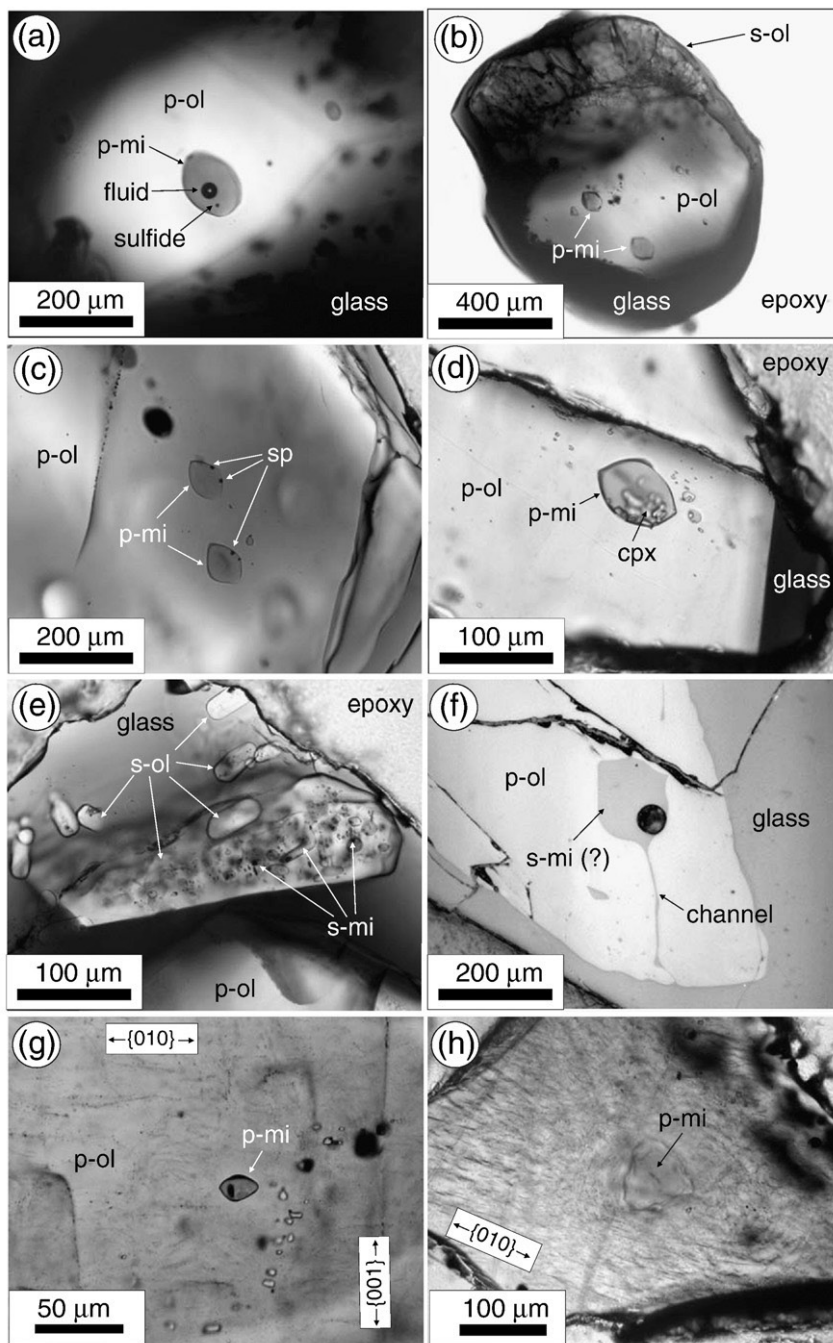


Fig. 1. Micrographs of natural melt inclusions in olivine and experimental products. (a) Primary melt inclusion in olivine from the Galapagos basalt surrounded by matrix glass; the inclusion consists of glass, a shrinkage bubble, a sulfide globule and a small crystal of chromium spinel. (b) Olivine (Fo₈₈) with primary melt inclusions after the experiment (run #248, inclusions MI-1 in Table 1); corona of secondary olivine surrounds upper rim of primary olivine crystal. (c) Primary inclusions in olivine (Fo_{87.5}) with after the experiment (run #263, inclusions MI-7a–b in Table 1); as in panel (b) inclusions contain homogeneous glass and tiny spinel crystals. (d) Primary inclusion in olivine (Fo₈₈) consisting of glass and several small crystals of high-Ca pyroxene, formed during the experiment (run #263, inclusions MI-6 in Table 1). (e) Secondary olivine crystals in matrix glass; large crystal hosts numerous melt inclusions and Fe-oxides (?) trapped during experiment. (f) Large secondary inclusion or, possibly, primary inclusion which leaked during the experiment; the inclusion is connected with the matrix glass by a thin channel (run #248, inclusion SMI-4). (g) Fragment of olivine from run #248 (MI-6) with numerous oxidation-decorated dislocations predominantly oriented along {001} and {010} planes. (h) Oxidation-decorated dislocations in olivine with melt inclusion from run #261 (ΔQFM+3.3, aH₂O=1). Note the change of preferred orientation of dislocations from parallel to {010} to concentrically centered on inclusion, which may result from a change of internal pressure in the melt inclusion during experimental homogenization. Abbreviations: *p-mi*—primary melt inclusion before or after experiment; *s-mi* secondary melt inclusion; *p-ol*—primary olivine; *s-ol*—secondary olivine, formed during experiment; *glass*—matrix glass; *sp*—spinel; *cpx*—high-Ca pyroxene. Photographs (a–e) and (g–f) are in transmitted polarized light; (f)—in reflected light.

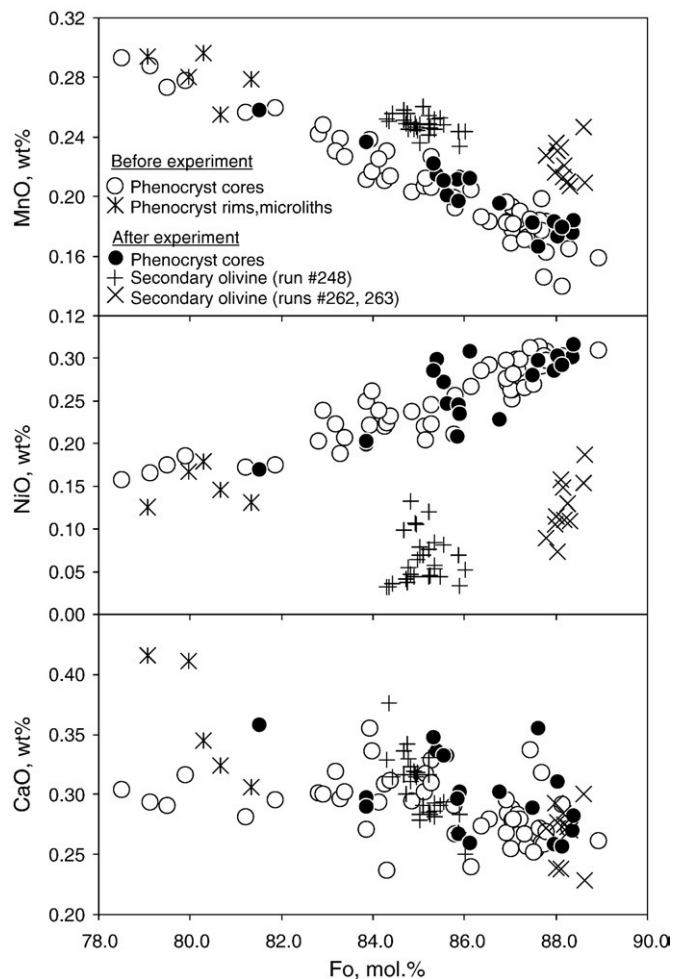


Fig. 2. Compositions of olivines before and after experiments. Note systematic difference between secondary olivines, which crystallized from matrix melt during experiments, and cores of primary olivines, which remained unchanged after experiments. This indicates that chemical equilibration with respect to major olivine components was not achieved between matrix melt and olivine cores hosting melt inclusions. Complete analyses of olivine are given in Supplementary Table 2.

rich rims of olivine phenocrysts were likely formed due to partial diffusive re-equilibration of the initially unzoned olivines of different compositions with evolved matrix melt prior to eruption. This may occur as a result of an injection of a new batch of melt in a magma chamber, which captures minerals from early-formed cumulates and transports them to the surface (Danyushevsky et al., 2002b).

Melt inclusions in olivine phenocrysts were glassy and typically contained brownish glass with or without shrinkage bubble, small sulfide globule, and occasionally small entrapped crystals of chromium spinel (Fig. 1a). The inclusions have variable compositions (Table 1, Supplementary Table 1) and were trapped by olivines at different stages of fractional crystallization of high-magnesian parental basaltic melt. Upon cooling at magmatic conditions, melt inclusions experienced crystallization of olivine on the inclusion walls and partial re-equilibration with the host olivines, which is testified by the symmetric zoning of olivine surrounding the glass inclusions and by the presence of sulfide globules in some glass inclusions (Fig. 1a) (Métrich et al., 1999; Danyushevsky et al., 2002a). Despite some variability in concentrations of major and trace elements, the water content measured by ion probe was nearly constant in all inclusions (0.46 ± 0.09 wt.%, 1 s.d., $n=16$) and similar to that in the matrix glass. The pre-eruptive pressure of the tholeiitic basalt is estimated from the matrix glass composition using olivine-pyroxene equilibria (Danyushevsky et al., 1996) to be about 100 MPa.

2.2. Experiments

Olivine crystals (0.5–1 mm in size) containing unexposed melt inclusions were loaded in $\text{Au}_{80}\text{Pd}_{20}$ capsules together with a powder of synthetic basaltic glass (Table 1). Eight to ten grains were loaded in every capsule. In run #248, the starting matrix material was composed of a dry glass (composition 140, Table 1) and 3 wt.% distilled water. In experiments #262 and #263 the matrix material was composed of pre-hydrated glasses with 2.8 and 3.6 wt.% H_2O , respectively (compositions 140-1 and 140-2, Table 1).

Experiments were conducted in vertically oriented internally heated pressure vessel (IHPV) at 200 MPa and 1140 °C for 48 h. This experimental temperature was chosen to be similar to the calculated liquidus temperature of melts in the natural glass inclusions ($\sim 1127 \pm 10$ °C, Table 1), which allowed simple evaluation of the effects of experimental treatment on the composition of inclusions. The IHPV was pressurized with Ar gas and all experiments were performed at the intrinsic redox conditions of the vessel. The $\text{Au}_{80}\text{Pd}_{20}$ capsules are permeable for H_2 and hydrogen fugacity in capsules was always buffered by the IHPV. Thus, the oxygen fugacity (f_{O_2}) in experimental charges was indirectly controlled by the fugacity of water through the equilibrium reaction $\text{H}_2 + 1/2 \text{O}_2 \leftrightarrow \text{H}_2\text{O}$. The intrinsic f_{O_2} prevailing in the IHPV at H_2O -saturated conditions (in the presence of pure H_2O -fluid, $a_{\text{H}_2\text{O}}=1$) was measured with Ni-Pd solid sensors (Taylor et al., 1992) and is equivalent to the value $\Delta\text{QFM}+3.3$ (3.3 log units above the Quartz–Fayalite–Magnetite oxygen buffer) (Schuessler et al., in press). Oxygen fugacities at water-undersaturated conditions in our charges were calculated following the procedure described in Scaillet et al. (1995). H_2O activities were evaluated from the concentration of dissolved water in silicate glass according to the model of Burnham (1979). Thus the prevailing oxygen fugacity in each capsule was estimated to be $\Delta\text{QFM}+2.6$ in the run #248 and $\sim\Delta\text{QFM}+2.4$ in the experiments #262 and #263 (Table 1). The second approach to estimate the oxygen fugacity during experiments was based on the assumption of equilibrium conditions ($K_d(\text{Fe}^{2+}-\text{Mg})=0.33$, Ford et al., 1983) achieved in the charges between matrix melt and secondary olivines (see Table 1 for details). The calculated values of oxygen fugacity are $\Delta\text{QFM}+2.0$ in run #248 and $\Delta\text{QFM}+2.5$ in experiments #262 and #263. Both estimates agree well for runs #262 and #263 and are within $10^{0.6}$ bars for run #248. The difference may reflect the uncertainty in hydrogen fugacity at intrinsic conditions in the IHPV.

After quenching, the mass preservation of experimental products was checked by comparing total weights of capsules before and after experiments, which agreed in all three runs within 0.6 mg ($\sim 0.1\%$ of total mass). The absence of the fluid phase in the capsules after experiments was checked by weighing the capsules, which were first punctured and then heated at 110 °C during 10 min.

One additional experiment (#261) was carried out by pressurizing natural olivines with pure water fluid ($a_{\text{H}_2\text{O}}=1$) under the same P–T conditions as the other experiments. However examination of mass preservation revealed leakage of water from the capsule. Despite this fact, we believe that the water escape from the capsule in run #261 took place during (or after) quenching, and olivines from this run have indeed experienced the treatment at experimental conditions in the presence of the pure H_2O fluid. This is demonstrated by the high H_2O contents in glass inclusion in olivine (Table 1). In addition, we also observed enhanced crystallization (hydrothermal growth?) of magnetite on the surface of the olivine grains, indicating that highly oxidized conditions were prevailing in the capsule (estimated oxygen fugacity was $\Delta\text{QFM}+3.3$ at $a_{\text{H}_2\text{O}}=1$, see above). Since the olivines were strongly oxidized during the run, their defect structure became visible (Fig. 1h).

2.3. Analytical methods

The experimental products were polished with diamond suspensions and finally with 0.05 μm corundum powder, studied under optical

Table 1
Composition of starting materials and experimental products

Sample # ^a	Starting compositions			Representative compositions of experimental products (200 MPa, 1140 °C, 48 h)																		
	Melt inclusions		Artificial matrix glasses	Run #248						Run #262					Run #263					Run #261		
	#140	#140-1	#140-2	MG	SMI-4	MI-1	MI-2	MI-3	MI-5a	MI-6	MG	SMI-1	MI-2a	MI-3	MI-5	MG	MI-3	MI-4	MI-6	MI-7a	MI-3	
Matrix glass				#140	#140	#140	#140	#140	#140	#140	#140-1	#140-1	#140-1	#140-1	#140-1	#140-2	#140-2	#140-2	#140-2	#140-2	No	
Free water added				3 wt.%	3 wt.%	3 wt.%	3 wt.%	3 wt.%	3 wt.%	3 wt.%	No	No	No	No	No	No	No	No	No	No	Yes	
SiO ₂ wt.% ^b	49.7 (12)	49.90	48.21	47.50	48.20	48.48	48.99	50.60	49.74	48.67	50.45	47.33	47.74	49.50	49.64	48.45	47.37	48.95	49.62	49.80	47.60	50.15
TiO ₂	2.5 (0.32)	1.01	1.01	1.02	1.08	1.10	2.03	2.24	2.25	1.84	1.73	0.94	1.02	2.09	1.75	2.04	1.00	1.98	2.15	1.77	2.24	1.64
Al ₂ O ₃	15.9 (1.2)	15.59	14.76	14.53	14.75	14.77	13.09	13.85	13.45	13.13	14.92	14.92	15.03	13.90	15.19	14.27	14.93	12.98	14.97	15.93	15.10	12.39
FeO	9.2 (1.3)	9.46	9.07	8.95	10.39	10.44	9.23	8.88	9.14	11.14	10.06	12.62	12.13	10.56	9.48	10.85	12.55	13.54	8.53	8.96	9.53	9.57
MnO	0.14 (0.03)	0.17	0.18	0.20	0.18	0.18	0.14	0.15	0.12	0.13	0.17	0.20	0.19	0.13	0.13	0.13	0.19	0.20	0.14	0.12	0.13	0.13
MgO	6.3 (0.3)	9.51	8.99	8.93	8.97	8.91	8.71	8.64	8.74	8.69	8.09	7.89	7.82	7.80	7.84	8.00	7.81	7.45	7.77	7.63	7.78	9.18
CaO	12.6 (0.7)	12.04	11.97	12.07	11.56	11.52	10.50	10.71	10.52	11.18	9.48	11.81	11.74	10.83	11.45	10.96	11.72	10.10	11.05	11.47	11.40	9.76
Na ₂ O	2.63 (0.18)	2.19	2.21	2.22	2.10	2.12	2.26	2.31	2.23	1.77	2.48	2.14	2.13	2.31	2.21	2.12	2.15	2.27	2.39	1.99	2.08	2.08
K ₂ O	0.34 (0.11)	0.06	0.07	0.07	0.07	0.07	0.27	0.28	0.31	0.18	0.31	0.07	0.07	0.33	0.29	0.30	0.07	0.40	0.34	0.38	0.33	0.22
S	0.09 (0.04)				0.01	0.00	0.06	0.10	0.07	0.06	0.06	0.00	0.00	0.10	0.11	0.09	0.01	0.04	0.07	0.04	0.11	0.07
Cl	0.02 (0.01)				0.01	0.02	0.01	0.02	0.02	0.00	0.01	0.01	0.01	0.01	0.01	0.01	0.01	0.02	0.01	0.01	0.02	0.01
Total	100.00	99.93	96.46	95.49	97.33	97.60	95.28	97.79	96.58	96.78	97.76	97.93	97.89	97.57	98.12	97.22	97.79	97.94	97.04	98.10	96.32	95.20
H ₂ O (KFT) ^c					2.55(0.06)							1.89(0.08)					1.73(0.09)					
H ₂ O (SIMS) ^d			2.80(0.04)	3.56(0.05)	2.60(0.01)	2.71	2.31	2.93	2.64	2.83	2.91	1.80(0.02)	1.42	1.82	1.82	1.74	1.82(0.02)	1.39	1.91	1.93	1.45	3.31
B, ppm ^d	1.51 (0.33)				0.73	2.58	1.20	1.06	1.42	0.85	1.30			1.08							0.88	0.87
Li	3.34 (0.53)				0.64	0.64	2.43	3.13	2.86	2.84	2.95			2.55							2.33	2.44
Be	0.78 (0.12)				0.10	0.11	0.70	0.89	0.83	0.59	0.53			0.74							0.49	0.65
F	548 (93)				60	89	249	340	313	220	202			370							210	321
K	3988 (670)				612	620	2158	2555	2614	1394	2488			2974							2868	1916
Cr	239 (47)				119	127	360	296	312	4351	367			191							872	226
Ti	17490 (2118)				6308	6275	11,537	13,657	12,833	10,943	9950			14,047							13,430	10,893
Sr	319 (31)				15	17	226	276	231	201	219			299							298	224
Zr	146 (28)				6	7	97.8	104	114	88	95			116							116	95
Ba	86 (13)				3.4	4.9	54.6	67.9	63.1	36.5	64.4			79.7							77.9	48.1
Nb	21.8 (4.1)				1.4	1.6	13.2	16.5	16.7	9.3	16.9			17.6							17.3	12.2
Y	26.3 (3.4)				0.8	1.0	20.5	23.1	21.7	19.8	17.1			22.3							18.3	18.2
V	343 (25)				43	45	259	285	294	344	238			291							296	243
La	12.8 (2.2)				0.6	0.7	9.41	10.8	10.1	7.3	11.0			12.1							11.1	8.0
Ce	31.7 (5.1)				1.0	1.2	24.0	24.6	26.2	19.2	23.1			27.8							28.1	20.3
Nd	18.6 (2.7)				0.6	0.6	14.3	16.3	15.3	13.9	14.2			16.9							15.1	13.1
Sm	5.03 (0.68)				0.16	0.24	3.97	4.24	4.15	3.78	3.34			4.41							4.64	3.37
Eu	1.65 (0.21)				0.05	0.06	1.30	1.62	1.37	1.45	1.29			1.47							1.49	1.09
Gd	5.34 (1.21)				0.27	0.11	4.19	4.76	5.27	4.16	4.02			5.38							5.01	3.19

Dy	4.66 (0.72)	0.17	0.16	3.69	4.25	3.95	3.98	3.15		4.17									3.72	3.36
Er	2.66 (0.38)	0.07	0.13	2.27	2.56	2.39	2.41	1.74		2.21									2.08	2.01
Yb	2.10 (0.32)	0.11	0.14	1.83	2.23	1.99	2.02	1.50		2.09									1.75	1.76
Pb	0.85 (0.23)	8.72	9.18	0.96	1.02	0.94	0.91	1.13		1.18									0.93	1.28
Th	0.82 (0.19)	0.06	0.06	0.58	0.87	0.84	0.66	0.87		0.81									0.78	0.61
U	0.26 (0.07)	0.03	0.02	0.21	0.24	0.27	0.22	0.28		0.24									0.21	0.20
Hf	3.31 (0.67)	0.18	0.15	2.67	3.06	2.72	2.25	2.54		2.73									2.69	2.44
T °C (Dry, 200 MPa) ^a	1149 (10)	1226	1224	1231	1226	1230	1215	1217	1200	1198	1207	1202	1209	1199	1199	1207	1192	1202	1202	1253
T °C (Wet, 200 MPa) ^b	1127(10)	1146	1142	1158	1139	1149	1130	1131	1140	1145	1146	1141	1149	1137	1149	1144	1128	1150	1158	
Olivine Fo, mol% ^c	85.3 (3.0)	88.1	87.5	88.0	88.4	88.1	85.4	86.1	85.2	85.4	85.6	87.6	85.8	85.0	81.5	88.4	88.0	87.5	88.8	
Mg# glass, mol% ^d	55.3 (4.0)	60.6	60.3	62.7	63.4	63.0	58.2	58.9	52.7	53.5	56.8	59.6	56.8	52.6	49.5	61.9	60.3	59.3	63.1	
K _d Mg-Fe (1) ^e		0.21	0.22	0.23	0.23	0.23	0.24	0.23	0.19	0.20	0.22	0.21	0.22	0.20	0.22	0.21	0.21	0.21	0.21	0.22
Fe ²⁺ /Fe _{total} ^f		0.63	0.63	0.64	0.62	0.63	0.62	0.62	0.59	0.60	0.59	0.59	0.59	0.59	0.61	0.59	0.59	0.61	0.59	0.61
K _d Mg-Fe (2) ^g		0.33	0.35	0.36	0.37	0.36	0.38	0.37	0.33	0.33	0.38	0.35	0.37	0.33	0.36	0.36	0.35	0.34	0.35	0.34
ΔQFM (1) ^h		+2.0	+2.0	+2.0	+2.0	+2.0	+2.0	+2.0	+2.5	+2.5	+2.5	+2.5	+2.5	+2.5	+2.5	+2.5	+2.5	+2.5	+2.5	+2.5
aH ₂ O ^k		0.60	0.63	0.59	0.77	0.69	0.79	0.68	0.35	0.24	0.39	0.34	0.35	0.35	0.29	0.37	0.35	0.23		
ΔQFM (2) ^l		+2.6	+2.6	+2.6	+2.6	+2.6	+2.6	+2.6	+2.4	+2.4	+2.4	+2.4	+2.4	+2.4	+2.4	+2.4	+2.4	+2.4	+2.4	+3.3
K _d Mg-Fe (3) ^m		0.37	0.40	0.41	0.42	0.41	0.43	0.42	0.32	0.32	0.36	0.34	0.36	0.32	0.36	0.35	0.34	0.34		

High Cr content of the inclusions MI-5a from run #248 (4351 ppm, italicized in table) is likely due to trapping small chromium spinel during ion-probe analysis.

^a MG—matrix glass, MI—melt inclusion, SMI—secondary melt inclusion;

^b Major elements (in wt.%) determined by electron probe. 1 s.d. of the mean values are in brackets;

^c H₂O in matrix glasses (in wt.%) determined by Karl-Fischer titration technique (Behrens and Stuke, 2003);

^d H₂O (in wt.%) and trace elements (in ppm) determined by ion probe;

^e Dry liquidus olivine temperature (in °C) estimated after (Ford et al., 1983);

^f Wet liquidus olivine temperature (in °C) estimated after model (Ford et al., 1983) and corrected for presence of water in melt after (Almeev et al., 2007). Except for one inclusion, the calculated liquidus temperature is identical to the experimental temperature within 10 °C, indicating that local equilibrium in the melt inclusions was attained and effective quenching prevented crystallization of olivine on the inclusion walls.

^g Composition of host olivine for melt inclusions (MI or SMI) or secondary olivine for matrix glasses (MG) (Fo=100 Mg/(Mg+Fe), mol%).

^h Glass Mg# = 100 Mg/(Mg+Fe_{total}), mol%.

ⁱ K_d Fe-Mg between olivine and melt, calculated assuming that all iron in the melt is as Fe²⁺.

^j Calculations of Fe²⁺/Fe_{total}, K_d Fe-Mg and oxygen fugacity ΔQFM (expressed as deviation of log(fO₂) from that of the QFM oxygen buffer at experimental conditions) assuming equilibrium conditions between matrix melt (MG) and secondary olivines in the experiments. Conventional K_d Mg-Fe = 0.33 (Ford et al., 1983) was used to calculate Fe²⁺/Fe_{total} in the matrix melt (0.63 and 0.59 in runs #248 and #262 and #263 respectively). Oxygen fugacity in the charges (ΔQFM¹²) was computed using Fe²⁺/Fe_{total}, melt H₂O content and melt composition using the model of Moretti (2005). The obtained values of oxygen fugacities were assumed to represent the prevailing fO₂ in individual charges (QFM+2 in the run #248 and QFM+2.5 in runs #262 and #263). These values of oxygen fugacity were further used to calculate Fe²⁺/Fe_{total} in melt inclusions, and K_d Fe-Mg between host olivines and melt inclusions using melt H₂O content and melt composition in the charges.

^k H₂O activity in melts calculated after Burnham (1979);

^l Oxygen fugacity in the charges (expressed as ΔQFM) was calculated following the procedure of Scaillet et al. (1995) using the known aH₂O in the melts (Burnham, 1979) and intrinsic oxygen fugacity in the IHPV. The oxygen fugacity in run #261 (aH₂O = 1) is assumed to be ΔQFM = +3.3. See also Feig et al. (2006) for details of calculations.

^m K_d Fe-Mg between matrix melts and secondary olivines and between melt inclusions and host olivines, calculated using oxygen fugacities ΔQFM(2).

microscope and with electron and ion probes. The major element concentrations in glasses (melt inclusions) and in olivine were analyzed using Cameca SX50 and JEOL JXA 8200 electron microprobes at IFM-Geomar (Kiel) at 15 kV. Glasses were analyzed at 10 nA over 5 to 10 μm areas. The analyses given in Table 1 are average values of 3 to 5 measurements for every melt inclusion, and of 20 to 30 measurements for matrix glass. The host olivine was analyzed at 30 nA with focused beam. Three analyses were performed around each inclusion at the distance approximately equal to that of the radius of the inclusion. Synthetic standards from Cameca and natural minerals and glasses (Jarosewich et al., 1980) were used for calibration. Counting time was 20/10 s (peak/background) for major elements, 60/30 s for K, S, and Cl. Basaltic glass VG-2 (USNM 111240/52) and San Carlos olivine (USNM 111312/444) were used as monitor samples in routine measurements of glasses and olivines, respectively (Supplementary Table 3).

The concentrations of water and trace elements in melt inclusions were determined by secondary ion mass-spectrometry (SIMS) using CAMECA ims4f at the Institute of Microelectronics (Yaroslavl', Russia) (Sobolev, 1996; Portnyagin et al., 2007). When analyzed, samples coated with a 30 nm thick gold film were bombarded by a primary beam of O^{2-} ions. The area for analysis was first sputtered for 3 min with 70 μm diameter beam to remove surface contamination. For analysis, the beam was focused to a spot 10–20 μm . The primary-ion energy was 14.5 keV at 15–20 nA current. The secondary ions ($^1\text{H}^+$, $^7\text{Li}^+$, $^9\text{Be}^+$, $^{11}\text{B}^+$, $^{19}\text{F}^+$, $^{30}\text{Si}^+$, $^{39}\text{K}^+$, $^{47}\text{Ti}^+$, $^{51}\text{V}^+$, $^{52}\text{Cr}^+$, $^{88}\text{Sr}^+$, $^{89}\text{Y}^+$, $^{90}\text{Zr}^+$, $^{93}\text{Nb}^+$, $^{138}\text{Ba}^+$, $^{139}\text{La}^+$, $^{140}\text{Ce}^+$, $^{149}\text{Sm}^+$, $^{153}\text{Eu}^+$, $^{154}\text{Gd}^+$, $^{156}\text{Gd}^+$, $^{158}\text{Gd}^+$, $^{163}\text{Dy}^+$, $^{164}\text{Dy}^+$, $^{167}\text{Er}^+$, $^{174}\text{Yb}^+$, $^{178}\text{Hf}^+$, $^{232}\text{Th}^+$, $^{238}\text{U}^+$, $^{208}\text{Pb}^+$) emitted from the sample were filtered by the high accelerating-voltage offset (~ 100 V, bandwidth ± 50 V) and analyzed at a mass spectrometer resolution of $M/\Delta M = 300$ in pulse-counting mode. Counting time was dynamically corrected for each element and varied between 5 and 120 s depending on current counting statistics. Single analyses are average values from 5 cycles of measurements. The total analysis time varied from 50 to 70 min. Secondary ion intensities were normalized to $^{30}\text{Si}^+$ and converted to weight concentrations using calibration curves based on a set of well characterized natural and artificial glasses (Sobolev and Chaussidon, 1996; Rocholl et al., 1997; Jochum et al., 2006). Correction of isobaric interferences was applied for Eu, Gd, Er and Yb following the technique described in Gurenko et al. (2005) and references therein. Accuracy and precision were estimated to be better than 10% for all elements with concentrations above 1 ppm and 10 to 30% for concentrations 0.1–1 ppm and $\sim 15\%$ for hydrogen. Detection limit for trace elements is estimated at 0.01–0.005 ppm. Background signal for $^1\text{H}^+$ converted to weight percent of water equivalent was 0.01–0.02 wt.% as measured on nominally anhydrous olivine phenocrysts from highly depleted MORB from Sequeiros Fracture Zone. The glasses KL-2G (Jochum et al., 2006) and NIST-610 (Rocholl et al., 1997) were used as daily monitors for trace element analyses (Supplementary Table 3).

Abundance and structural position of hydrogen and water in olivines prior and after experiments were studied by means of Fourier Transform Infrared spectroscopy (FTIR) at the University of Alberta (Edmonton). Olivine grains were cut and polished from both sides to produce 200 μm thick platelets. The polished grains were mounted in the Continuum infrared microscope attached to the Thermo Nicolet Nexus 470 FTIR spectrometer. Both spectrometer bench and IR optics of the microscope were continuously flushed with dried air in order to minimize spectral noise due to air humidity. FTIR spectra were collected using unpolarized IR beam in transmission mode. Aperture size was $50 \times 50 \mu\text{m}$. 200 to 400 scans were collected for each measurement. Orientation of the beam relative to the olivine crystal structure was determined using 2nd order Si–O overtone (Jamtveit et al., 2001). Spectra acquired with beam direction close to [010] axis were used to calculate water concentrations. In order to avoid non-systematic uncertainties in hydroxyl absorbance due to partial polarisation of nominally non-polarized beam in the optics of IR microscope (Libowitzky and Rossman, 1996) the water concentration in olivine was calculated from eight FTIR spectra. Sample stage was rotated by 45° before each spectrum acquisition. Acquired spectra were

baseline corrected using 3rd order polynomial fit using OMNIC software supplied with the FTIR spectrometer. OH bands were integrated and H_2O concentrations were calculated using the method based on formulae from Paterson (1982) and calibration of Bell et al. (2003). The details of the method are given in Matveev and Stachel (2007).

3. Results

The experimental products consisted of homogeneous hydrous glass (1.8–2.6 wt.% H_2O , Table 1), olivine crystals with melt inclusions and newly formed small olivine crystals. Asymmetric overgrowths of secondary olivine on primary olivines (Fig. 1b, e) were also observed. No fluid bubbles were found in the glass, suggesting that the matrix melt was water-undersaturated at the experimental conditions. The composition of the newly formed secondary euhedral olivine crystals (typically 20–50 μm in size, Fig. 1e) was $\text{Fo}_{87.8-88.6}$ in run #248 and $\text{Fo}_{84.3-85.9}$ in runs #262 and #263 (Fig. 2, Table 1, Supplementary Table 2). The secondary olivines have higher MnO content; lower NiO and similar CaO compared to primary olivines at equal Fo-number. Elevated MnO/FeO in the secondary olivines can be explained by slightly higher MnO/FeO in our synthetic glasses (0.018–0.022) compared to natural melts (~ 0.015) and also by more oxidizing conditions in our experiments, which resulted in increasing MnO/FeO ratio in melts due to Fe oxidation. Low NiO in secondary olivines reflects crystallization from nominally Ni-free synthetic matrix melts contaminated by a small amount of natural Ni-rich olivine dissolved during experiments.

The compositions of olivine cores did not change significantly during the experiments. They range from Fo_{81} to Fo_{88} and have concentrations of minor components (Ni, Mn, Ca) well within the range of natural olivines prior to experiments (Fig. 2). An effect of the experimental treatment on the composition of the primary olivines was only observed near the rim of the minerals over a $\sim 200 \mu\text{m}$ zone. In this zone the natural normally zoned rim of crystals was replaced with newly formed more magnesian rim, where compositions changed gradually (from rim toward center) from Fo values in equilibrium with matrix melt (Fo_{85-88}) to the Fo values of cores of starting olivines. Inverse zoning was developed at rims of olivines which core compositions were less magnesian than olivines in equilibrium with matrix melt (Fig. 3).

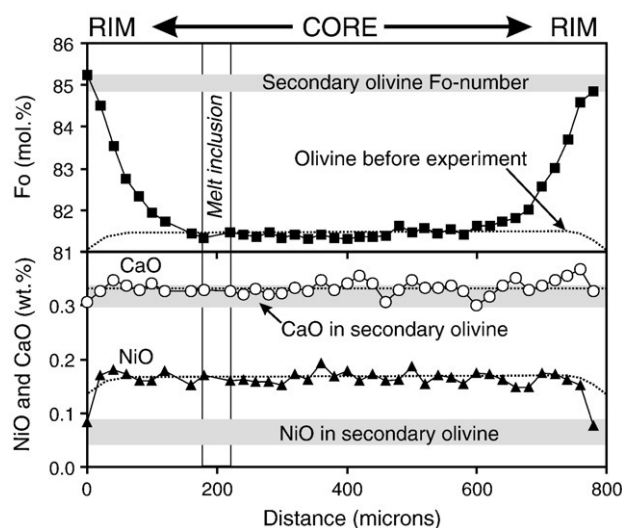


Fig. 3. Compositional profile across an olivine crystal after experiment (grain with inclusion MI-3 from run #263, Table 1). Fe–Mg exchange between olivine and matrix melt during experiment produced gradually increasing Fo compositions toward the crystal–melt interface. The diffusion zoning of trace elements (CaO and NiO) in olivine was not developed. Horizontal shadowed fields denote the range of secondary olivine composition from run #263 equilibrated with the matrix glass. Dotted line illustrates compositional zoning of the crystal before experiment, suggested on the basis of data on chemical zoning in olivines from the studied sample. The profile passed near to a melt inclusion, which position is shown by the vertical lines.

Noticeably, the diffusive zoning at the olivine rims is significantly wider for Mg and Fe (~200 μm) compared to that of micro elements (e.g., Ni, <50 μm) (Fig. 3). Diffusivities of Ni and Fe–Mg in olivine are similar at dry conditions and equally dependent on oxygen fugacity (e.g., Petry et al., 2004). Decoupling of these elements in our experiments can be explained if high water pressure and incorporation of protons in olivine structure (see below) accelerated significantly Fe–Mg exchange (Hier-Majumder et al., 2005) but had little effect on Ni diffusion. Previous experimental study showed that at relatively oxidizing conditions Ni negatively correlates with hydroxyl in olivine structure (Matveev, 1997). Ni-rich (~20 wt.% NiO) olivines were found to be incapable of storing structurally bonded OH in spectroscopically detectable amounts. Perhaps, Ni diffusion is largely independent on $f_{\text{H}_2\text{O}}$ since Ni is excluded from hydrogenation reactions. This observation needs attention in the future studies.

FTIR investigations of the olivine crystals hosting inclusions revealed significant changes after experimental treatment. The crystals of olivine were nearly dry olivines (<10 ppm H₂O) before experimental treatment (Fig. 4). The concentration of water bounded in olivine structure as hydroxyl groups also increased significantly, up to ~40–50 ppm H₂O for runs #262 and #263 and ~60 ppm in run #248 (Fig. 4). The apparent partition coefficient of structurally bond water between olivine and matrix glasses ($D_{\text{H}_2\text{O}}=0.0022\text{--}0.0027$), calculated from these data, is in good agreement with previous results (Koga et al., 2003; Aubaud et al., 2004), suggesting that equilibrium between olivines and matrix melt was attained with respect to water. Noticeably, intensity of OH IR bands increased, while their positions and proportions remained roughly the same as in the starting olivine as olivine structure became hydrogenated during experiments (Fig. 4).

Oxidation-decorated dislocated structure of the studied olivines could be observed in all runs and was particularly well developed at highly oxidized conditions in run #261, when olivines interacted with pure water fluid. The oxidation was mainly concentrated along discontinuous planes subparallel to {010} and along rare cracks (cleavage) parallel to {001} (Fig. 1g). The amount and occurrence of these planes were found to be unrelated to the presence of melt inclusions in most olivines. In one grain, we observed the change of the predominant orientation of the oxidation-decorated planes to concentrically orient around melt inclusion (Fig. 1h). Olivine spectra acquired in the regions of abundant dislocations displayed very strong

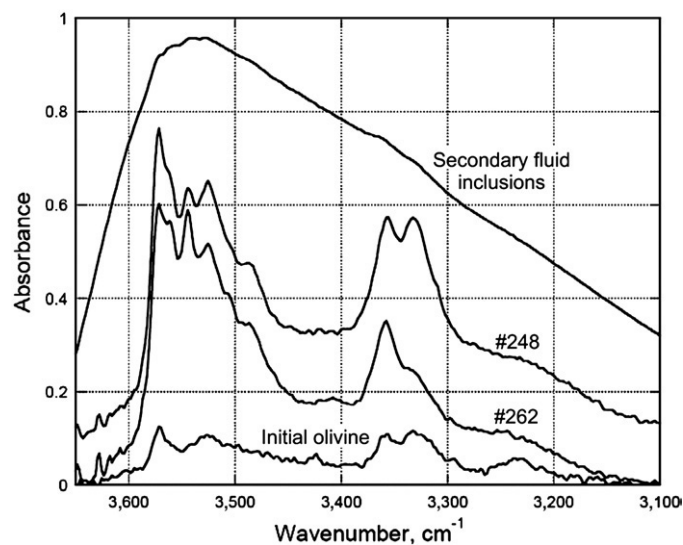


Fig. 4. Representative FTIR spectra of OH in olivines illustrating hydration of olivines during experiments. Bottom to top: before experiment; after run #262, after run #248. The upper spectrum as a typical spectrum of molecular water measured on areas rich in fluid inclusions. All spectra (except the spectrum of molecular water) are normalized to 1 cm thickness and stacked for clarity. In order to compare the spectrum of molecular water with OH absorption spectra of olivine, its intensity was reduced by a factor of 12.

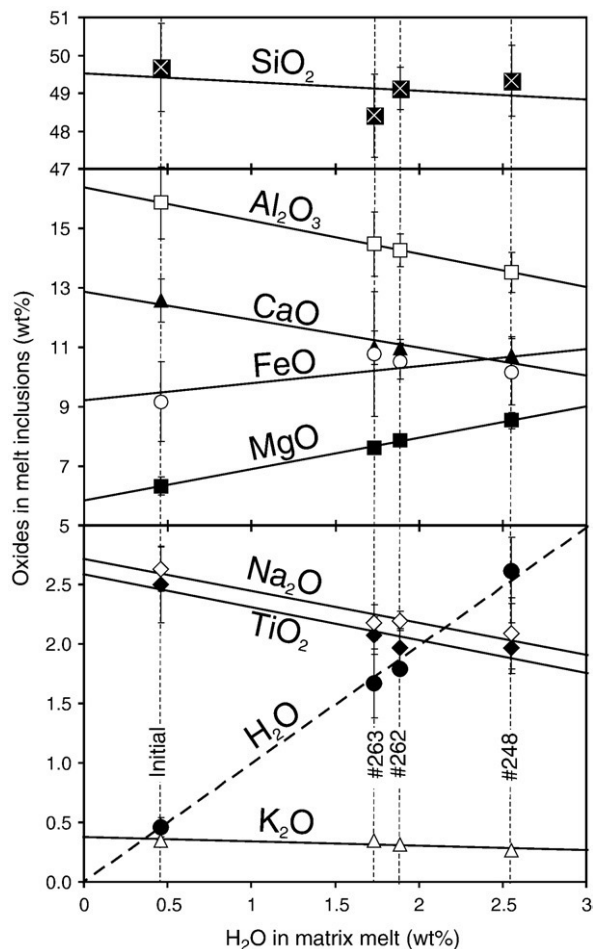


Fig. 5. Variations of the major elements in melt inclusions before (mean composition) and after experiments (mean compositions for runs #248, 262 and 263) plotted against H₂O content in matrix glasses. Note the complete re-equilibration of inclusions with matrix glass with respect to H₂O (linear least-square regression going through the origin). Other major elements changed systematically in order to maintain hydrous equilibria with olivine: MgO in melt increased, SiO₂ and FeO remained nearly constant, elements incompatible in olivine (CaO, Al₂O₃, Na₂O, TiO₂, K₂O) decreased proportionally to the amount of dissolved olivine. Error bars correspond to 1 standard deviation of the mean values for inclusions from every run.

absorbance bands of molecular water (Fig. 4), which is assigned to the presence of numerous tiny fluid inclusions.

Most primary inclusions did not show any evidence for leak (Fig. 1b–d) after the experimental treatment. However, the shape, the modal and chemical compositions of the inclusions changed significantly after the experiment. The typical oval or rounded shape of natural inclusions (Fig. 1a) has transformed in many cases to negative olivine crystal shape; fluid bubbles and sulfide globules disappeared (Fig. 1b–c). Small crystals of high-Ca pyroxene crystallized in some inclusions and were particularly common in runs #262 and #263 (Fig. 1d). Micron-sized chromium-bearing spinel unmelted during experiments also occurred in many inclusions (Fig. 1c). In comparison to untreated inclusions, the most pronounced compositional variation was observed for H₂O, with an increase by a factor of 3–5 (up to 1.4–2.9 wt.% in runs #248, 262 and 263). Up to 3.3 wt.% H₂O was measured in melt inclusion from run #261 (Fig. 1h), where olivines were pressurized with pure water fluid (Table 1). The compositions of the experimental products from this run are however not discussed in detail here because of unsatisfactory mass preservation (Section 2.2).

Although the range of measured water concentrations in melt inclusions from every run (e.g., from 2.3 to 2.9 wt.% in inclusions from run #248) exceeded the analytical uncertainty, we found no correlation between this water content and the size of inclusions or the position of

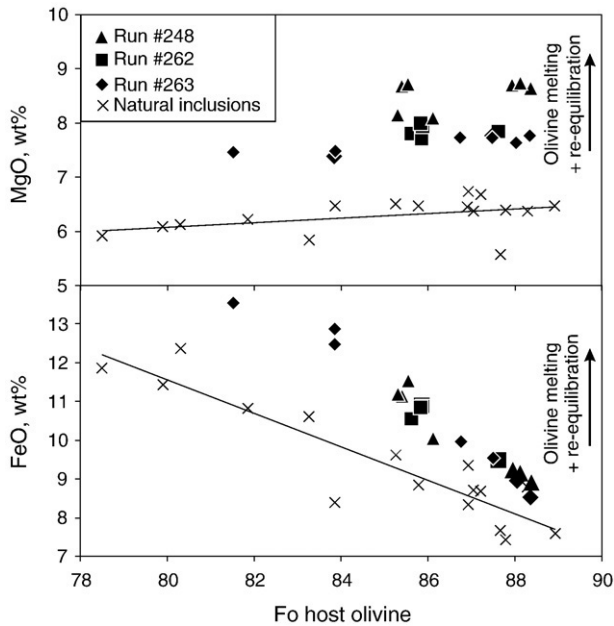


Fig. 6. Concentrations of MgO and FeO in melt inclusions before (crosses) and after experimental treatment (solid symbols). The composition of host olivine remained unchanged. The least-square linear regression line drawn for the compositions of unheated inclusions is shown for reference. Arrows illustrate effect of H₂O addition on equilibrium melt composition in olivine-hosted inclusion, which results from melting of olivine followed by Fe–Mg re-equilibration. For further discussion, see text.

inclusions in olivine crystals. The average water content of the analyzed heated glass inclusions was similar to that of the matrix glasses (Fig. 5) suggesting that complete re-equilibration of matrix glasses and melt inclusions with respect to water was achieved during our experiments.

The MgO concentration in heated inclusions increased by ~1.5 wt.% (to 7.4–8 wt.%) in runs #262 and 263 and by ~2 wt.% (to 8.1–8.7 wt.%) in run #248, which implies melting of olivine from inclusion walls during experiments. The FeO concentrations in the heated inclusions (8.5–13.5 wt.%) strongly correlate with Fo of host olivine and are up to 1–2 wt.% higher compared to unheated inclusions enclosed in olivine of similar Fo

content (Fig. 6). The FeO and MgO in the heated inclusions increased in proportion FeO/MgO ~ 0.5–1.7. This ratio is significantly higher compared to the stoichiometric FeO/MgO olivine ratio (0.23–0.40 for Fo_{81.5–88.4}) and implies that melting of the host olivine was accompanied by Fe–Mg exchange between inclusions and host olivine. Calculated K_d Fe²⁺–Mg between melt inclusions and their host olivines (0.34–0.43, Table 1) are close to the equilibrium values (0.33 ± 0.03, Ford et al., 1983) and interpreted as evidence for significant Fe–Mg re-equilibration of the inclusions with their hosts. More precise quantification of the extent of Fe–Mg re-equilibration is limited due to the uncertainties with determination of the oxygen fugacity in the inclusions, unknown initial composition of the inclusions and unknown composition of olivine on the inclusion walls melted during experiments.

The concentrations of other major elements (Ca, Al, Ti, Na), the majority of trace elements (e.g. K, REE) and sulphur, which are incompatible with respect to olivine, decreased in the heated glass inclusions after experiments (Figs. 5, 7). The concentrations of incompatible trace elements remained however in a marked contrast compared to the trace element pattern of the synthetic matrix glass (Fig. 7). The bulk amount of olivine components incorporated into melt inclusions during experiments was estimated from comparison CaO concentrations in natural and heated inclusions to be on average ~14% relative for run #248 and ~11% relative for runs #262 and 263 (Fig. 5). The decrease of trace element concentrations, except Pb and F, was within uncertainty of the average estimates similar to that calculated from Ca concentrations (Fig. 7, Table 1). Lead concentrations, which were very high in matrix melts (~9 ppm), increased slightly in melt inclusions after experiments. Fluorine concentrations in inclusions, in opposite, decreased by about a factor of two. The secondary inclusions trapped in olivine and formed during the experiments or the inclusions which exhibited signs of leakage (Fig. 1f) had compositions indistinguishable from that of the matrix glasses with respect to all major and trace elements (Table 1, Fig. 7).

4. Discussion and implications

4.1. Melt inclusions as a semi-closed system

The results presented in this study imply that melt inclusions in olivine behave as semi-closed system. Complete re-equilibration of

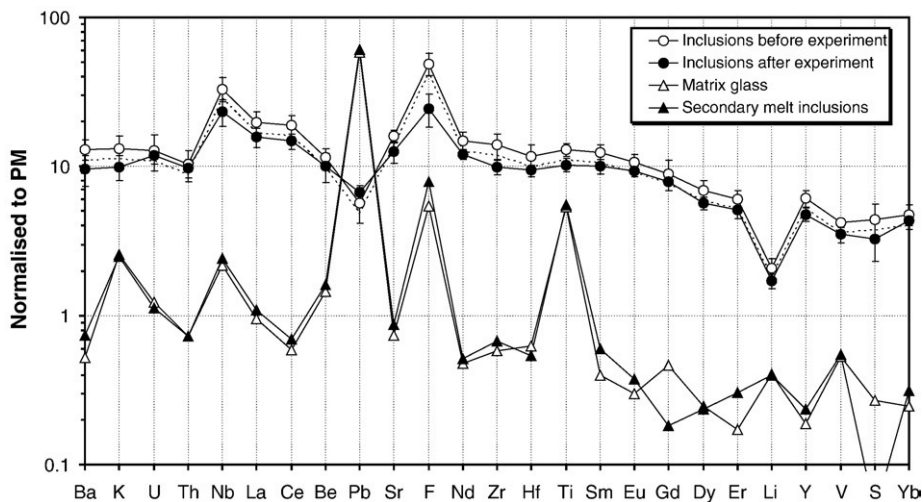


Fig. 7. Normalized concentrations of incompatible trace elements in melt inclusions and matrix glass (normalization to the composition of primitive mantle PM, Sun and McDonough, 1989). Note the large difference between primary melt inclusions and matrix glass. Leaked inclusion and secondary melt inclusions have the same composition as the matrix after experiment. The systematically lower concentrations of trace elements in the inclusions after experiment when compared to the initial compositions are explained as the result of melting of olivine during the experiment. Dotted line illustrates the effect of addition of 15% olivine to the average composition of unheated inclusion. The synthetic matrix glass should be nominally trace element free (except for TiO₂ which was added to the oxide mixture). However, the trace element pattern of the matrix glass is subparallel to that of the inclusions before experiment, indicating a small contribution of natural melt, which probably remained on the surface of olivine grains (most element concentrations can be interpreted by a contamination of less than 5 wt.% natural glass from Galapagos basalt). The very high Pb concentrations in the matrix glass are due to contamination during experiment (Pb may be incorporated in the noble metal capsules). Error bars correspond to 1 standard deviation of the mean values.

water between melt inclusions in large crystals (~1 mm in size) and matrix melt was achieved in 2 days during our experiments, which is several orders of magnitude faster than was expected before (Qin et al., 1992; Sobolev and Chaussidon, 1996; Danyushevsky et al., 2002a). Considering that the melt inclusions were completely re-equilibrated with matrix melt with respect to water during the experiments (Fig. 5), a minimum apparent diffusion coefficient for water can be estimated. We calculated the water diffusivity using the model of diffusive re-equilibration of melt inclusions and surrounding melt proposed by Qin et al. (1992). Partition coefficient of water between olivine and melt was assumed to be ~0.002 according to Aubaud et al. (2004), Koga et al. (2003) and data from this study. Assuming that 95% re-equilibration of 50 µm inclusion in the center of 1 mm crystal is obtained in less than 2 days, the apparent diffusion coefficient of H₂O is found to be $\geq 5 \times 10^{-12}$ m²/s at 1140 °C. The estimated diffusivity is nearly as fast as proton-vacancy diffusion (Mackwell and Kohlstedt, 1990) and is at least 3–4 orders of magnitude faster than for other major and trace elements at dry or hydrous conditions (Jurewicz and Watson, 1988; Chakraborty, 1997; Hier-Majumder et al., 2005; Spandler et al., 2007).

Other elements in melt inclusions, which exhibit anomalous behavior and could re-equilibrate partially with matrix melt, are lead and fluorine. With respect to fluorine, the observed 2-fold decrease of its concentrations in melt inclusions after experiment can probably be attributed to ~50% re-equilibration with matrix melt. In this case, fluorine ions had to move through olivine from F-rich inclusions to F-poor matrix melt, that is, in direction opposite to water. The apparent rate of the fluorine exchange in our experiments is surprisingly fast compared to other trace elements. This result however needs to be proved by longer experiments.

Lead concentrations are slightly higher in heated inclusions and can be explained if this element migrated through olivine from Pb-rich matrix melt to Pb-poor inclusions. Alternatively, elevated Pb concentrations can be explained if significant fraction of bulk Pb in natural inclusions was accommodated in sulphide globules, which melted during experiment and caused Pb concentrations in melts to increase. The Pb/Ce ratios in heated inclusions (on average Pb/Ce ~24.6) are indeed closer to typical mantle values (Pb/Ce ~25, Hofmann, 1997) than in unheated inclusions (Pb/Ce ~37). The Galapagos inclusions are not expected to have anomalously high Pb/Ce ratios, and thus the melting of sulphide provides a reasonable explanation for the increased Pb concentrations in heated inclusions. Although we do not favor diffusive re-equilibration of Pb between inclusions and matrix melt in this study, the anomalous behavior of this element as well as fluorine needs attention in future experimental studies.

Summarizing these results, we conclude that despite the complete re-equilibration of the system with respect to water, no or only partial re-equilibration was achieved with respect to major and trace elements between matrix melt, olivines and melt inclusions. An interaction of melt inclusion-bearing olivine phenocrysts with magma of different composition, which we simulated in this experimental study, is common in nature (Sobolev, 1996; Danyushevsky et al., 2002a). Therefore the water determinations in glass inclusions in olivine need to be interpreted with caution. Our results suggest that measured water concentrations in melt inclusions may not reflect the initial water contents or the minimum water concentrations as it is usually postulated (Sobolev and Chaussidon, 1996; Danyushevsky et al., 2002a; Wallace, 2005). The water concentration in melt inclusions in olivine may reflect the last equilibration event with the surrounding magma so that the determined water content in melt inclusions can be lower or higher than that of the melt at the time of entrapment. In light of our results, water gain or loss in olivine-hosted inclusions are very difficult to trace with the help of other, more slowly diffusing major and volatile elements. Several examples, which illustrate selective re-equilibration of natural inclusions with respect

to water, are described in Section 4.3. This process is anticipated to be particularly important during the evolution of the most primitive melt inclusions with presumably long residence time in magmatic system compared to evolved inclusions formed shortly before eruption.

4.2. Mechanisms of water transport through olivine

The proton diffusion in olivine is known to be very fast (Mackwell and Kohlstedt, 1990) and is interpreted to be the main mechanism responsible for rapid water loss from melt inclusions (Sobolev et al., 1989; Danyushevsky et al., 2002a; Hauri, 2002). The proton diffusion can be an equally important mechanism for water transport into melt inclusions if the external water pressure exceeds that in melt inclusions (Danyushevsky et al., 2002a).

It was suggested that the magnitude of water loss via water dissociation and proton diffusion is controlled by the oxidation of Fe in melt (Sobolev et al., 1989):



The same reaction can also account for a reduction of Fe and can, in principle, explain a water gain (Danyushevsky et al., 2002a), as required in our case. However, the water gain is limited by the ability of the melt to be reduced. As Fe³⁺ is the main component of natural melts that can be reduced, the maximum amount of H₂O that may be formed is:

$$\Delta\text{H}_2\text{O}(\text{wt.}\%) = 0.113 \times \text{Fe}_2\text{O}_3(\text{melt, wt.}\%).$$

For our experimental melts and basaltic melts in general, the amount of additional H₂O which can be accommodated by this reaction should be less than 1 wt.% (Danyushevsky et al., 2002a). Obviously, this amount is too small to explain our experimental data, indicating rather oxidized conditions (Table 1) and ~2 wt.% increase of the water concentration in the melt inclusions after experiment.

It seems that proton diffusion alone can hardly explain the large amount of water which inclusions gained during our experiments. An alternative or additional process, which could be involved, is a transport of molecular water through the lattice defects and micro-cracks in olivine. A highly dislocated structure of the studied olivine crystals is evident from optical observations of olivines after our experiments (Fig. 1g, h). The strong absorbance peak of molecular water in FTIR spectra of olivines (Fig. 4) ascribed to the presence of tiny fluid inclusions also strongly suggests that incorporation of molecular H₂O into olivines indeed took place during experiments. In previous studies conducted to achieve homogenization at 1 atm, water migration along dislocations or propagation of defect points in the host olivine were proposed to be the mechanisms explaining large water loss from inclusions (Massare et al., 2002). Similar processes are believed to be responsible for the selective water loss from fluid inclusions in quartz (Bakker and Jansen, 1994). Since the transport of molecular water into or from melt inclusion does not involve a chemical reaction affecting the redox state of melt components, the amount of water which can be transferred to inclusion should only be limited by the external water pressure and the amount of dislocations in host mineral. Hydrogen isotope fractionation in melt inclusion should be rather weak in this case (Hauri, 2002).

An important question is whether or not special conditions were created during our experiments, which caused the formation of numerous dislocations in olivine and accelerated water transport. One possibility is that the internal pressure of inclusions changed strongly during the experimental treatment, which may have caused extensive deformation of surrounding olivine and facilitated water transport. In some cases, we observed a change of the predominant orientation of oxidation-decorated dislocations in olivine from planes parallel to {010} to surfaces oriented concentrically around inclusion (Fig. 1h). This observation can be explained by re-crystallization of olivine and re-

orientation of dislocations due to changes of internal pressure in the inclusion. It is however evident from optical observations that the amount of dislocations did not increase significantly around inclusions compared to olivine far from the inclusion. Moreover significant pressure excess in melt inclusions during homogenization would not be possible without addition of H₂O to melt because the experimental temperature was chosen to be similar to the liquidus temperature of the natural inclusions. The deformed olivine structure around some inclusions can be rather a consequence of water addition to melt but not a major reason for the rapid water transport observed in our experiments.

Although we can miss some processes which are specifically related to the experimental procedure used in this study, our preferred explanation for the analytical data is that the dislocated olivine structure was likely an intrinsic feature of the olivines, as a consequence of non-ideal conditions of growth, and was not caused by micro-fracturing during natural cooling or by experimental treatment. During our experiments these dislocations were reactivated and served as pathways for the rapid water transport.

On the other hand, one may suggest that relatively oxidized conditions of our experiments caused rapid water diffusion. This might be the case if vacancy-controlled diffusion played a major role for the water transport due to increasing Fe³⁺ content in the olivine (Berry et al., 2007). Water incorporated in olivine at defect sites associated with trivalent cations causes absorption bands in olivine FTIR spectra in the wavenumber range between 3300 and 3400 cm⁻¹ (Berry et al., 2007). However, hydroxyl gained in the course of our high pressure experiments was largely associated with increased intensity of OH absorption bands located at higher frequencies, particularly in the wavenumber range between 3450 and 3600 cm⁻¹. Thus increasing Fe³⁺ concentration in olivine due to oxidation, which could be in part responsible for increased intensity of OH absorption bands in the 3300–3400 cm⁻¹ wavenumber range, was not a primary mechanism of OH dissolution in olivine. Therefore relatively high fO₂ in our experiments should not significantly affect dynamics of water exchange between inclusions and matrix melt.

4.3. Re-equilibration of inclusions at magmatic conditions

Our results imply that melt components with similar behavior during mantle melting or deep fractionation in the crust (e.g. H₂O and Ce or K₂O) (Michael, 1995; Sobolev and Chaussidon, 1996) can fractionate due to their different diffusivity in olivine during partial re-equilibration of melt inclusions. This provides alternative explanation for decoupling of water from incompatible trace elements and other volatiles (e.g. Cl and S) in suites of co-genetic primitive melt inclusions from mid-ocean ridge (Fig. 8a) and subduction zone (Fig. 8b) settings. Several studies including our new results on the composition of melt inclusions from the Galapagos basalt demonstrate that melt inclusions in high-Fo olivines typically have water concentration similar to matrix glass (Sobolev and Chaussidon, 1996; Portnyagin et al., 1997; Kamenetsky et al., 1998) (Fig. 8). Melt inclusions from some of the samples exhibit a large range of trace element concentrations, including melts of ultra-depleted composition (e.g., K₂O < 0.01 wt.%). Highly incompatible trace elements, Cl and S correlate usually well in these suites, but water content in melt inclusions is relatively constant for every particular sample. The apparent decoupling of H₂O and trace elements in the primitive melt inclusions, but not in MORB glasses (Michael, 1995), was explained by the presence of a H₂O–CO₂-bearing fluid phase during magmatic fractionation at mid-ocean ridges or by the presence of water-rich fluid in the source region in subduction zones (Sobolev and Chaussidon, 1996). An alternative mechanism to buffer water concentrations in melt inclusions is the re-equilibration of variably H₂O-depleted inclusions in olivine with matrix melt. This explanation was proposed by Kamenetsky et al. (1998) and is strongly supported

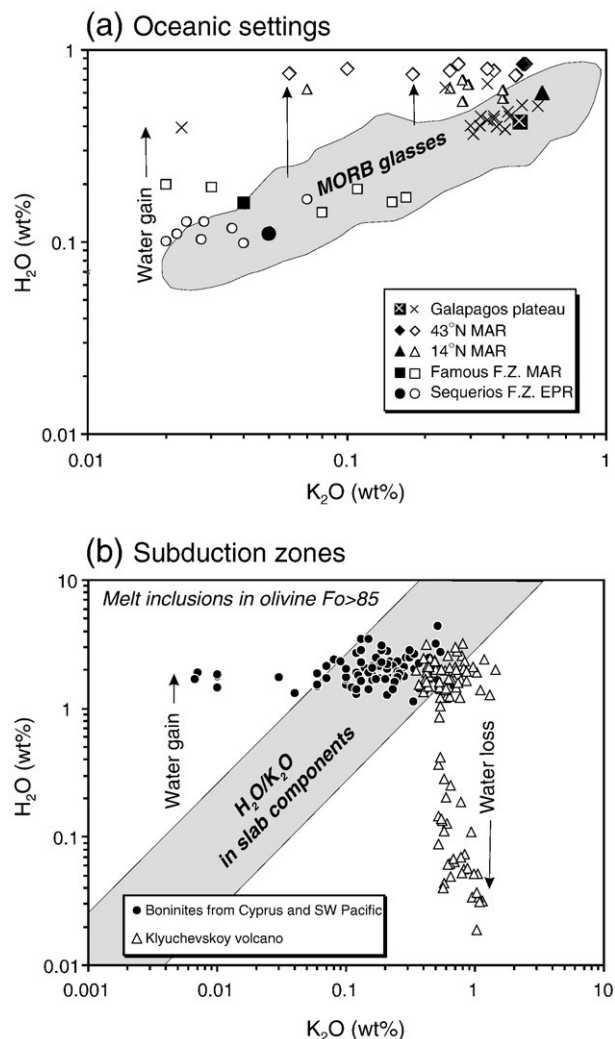


Fig. 8. Variations of H₂O and K₂O in primitive melt inclusions (host olivine Fo₈₅) from oceanic (a) and subduction-related (b) settings. Shown are data on melt inclusions in primitive olivines from the Galapagos Plateau (this study, Supplementary Table 1); 14°N and FAMOUS Fracture Zone of the Mid-Atlantic Ridge, Sequerios Fracture Zone at the East Pacific Rise (Sobolev and Chaussidon, 1996); 43°N of the Mid-Atlantic Ridge (Kamenetsky et al., 1998); boninites and primitive arc tholeiites from Cyprus and southeastern Pacific arcs (Sobolev and Chaussidon, 1996); Klyuchevskoy volcano in Kamchatka (Portnyagin et al., 2007; Sobolev and Chaussidon, 1996; Churikova et al., 2007). The field of MORB glasses in panel (a) is shown for comparison (Sobolev and Chaussidon, 1996). In figure (a) open symbols denote compositions of melt inclusions, closed symbols – matrix glasses. In panel (b) the grey field represents the range of H₂O/K₂O ratios (3–25) of water-bearing slab-derived melts or fluids, which should be observed in primary arc-magmas (Portnyagin et al., 2007; Eiler et al., 2000; Stolper and Newman, 1994). The horizontal trends towards the field with high H₂O/K₂O ratios in suites of inclusions from oceanic settings (a) and boninites (b) are interpreted to be the result of partial re-equilibration of low-H₂O low-K₂O inclusions with relatively H₂O-rich matrix melts. The vertical trend of Klyuchevskoy volcano inclusions towards the field with low H₂O/K₂O ratios suggests a nearly complete H₂O loss from inclusions during eruption and slow cooling.

by our new data. In this case, Fe–Mg disequilibrium of olivine phenocrysts and matrix glass does not rule out the possibility of re-equilibration of inclusions and matrix melt with respect to H₂O, since we illustrate in our study that water transport through olivine is faster than Fe–Mg exchange (Figs. 2, and 3).

The described examples of melt inclusions, which have likely re-equilibrated with matrix melt with respect to water, were trapped in very primitive olivines (>Fo₈₅) with presumably long residence time in the magmatic system. If the olivines with inclusions are not erupted shortly after crystallization, a change of water concentration in such

melt inclusions is expected to occur during subsequent magma evolution, as the result of an increase of water in matrix melt with ongoing fractionation or magma mixing.

4.4. Water loss from inclusions

Magma decompression at shallow depths may result in a significant H₂O loss from inclusions trapped in minerals at greater depth, which was proposed to occur via proton diffusion (Danyushevsky et al., 2002a; Wallace, 2005). However, the proton diffusion can hardly explain large amount of water lost from some natural melt inclusions or during experimental reheating. For example, Churikova et al. (2007) reported extremely low H₂O concentrations (mostly below 0.1 wt.%) in melt inclusions from the Klyuchevskoy volcano (Kamchatka), while other authors found H₂O concentrations as high as 3.5 wt.% in melt inclusions from the same localities and in olivines with similar Fo content (Sobolev and Chaussidon, 1996; Portnyagin et al., 2007) (Fig. 8b). All inclusions in olivines from Klyuchevskoy volcano are geochemically similar and the large variations in H₂O content cannot be explained by a compositional variability of parental melts (Portnyagin et al., 2007). A detailed examination of the rock types studied by the different authors is helpful to explain the large variation in water concentrations. All Klyuchevskoy olivines hosting low-H₂O inclusions were separated from massive lava flows, which cooled slowly after eruption (Churikova et al., 2007). Olivines hosting high-H₂O inclusions were separated from pyroclastic rocks (lapilli and volcanic bombs) which solidified rapidly (Sobolev and Chaussidon, 1996; Portnyagin et al., 2007). This observation indicates that a slow cooling at atmospheric pressure can probably lead to a nearly complete water loss from inclusions in olivine. Noticeably, the water loss is not accompanied by a strong oxidation of melt inclusions since many Klyuchevskoy inclusions with low H₂O content contain sulfide globules and exhibit no magnetite precipitates (Churikova et al., 2007). As proton diffusion cannot explain the dramatic water loss from slow cooling inclusions, an alternative explanation is a transport of molecular water through dislocations in olivine, which we favor in this study. A similar explanation was proposed previously to explain large water loss from hydrous inclusions during re-homogenization experiments at 1 atm pressure (Massare et al., 2002).

4.5. When is water in melt inclusions informative for magmatic conditions?

The rapid response of melt inclusions to variations of external water pressure implies that a careful selection of samples is a prerequisite for melt inclusion studies devoted to trace the water activity during magma evolution. If the history of olivine phenocrysts cannot be reconstructed adequately, a statistically significant correlation between water, other volatile components (e.g., S and Cl) and incompatible trace element concentrations should serve as a good argument for the preservation of the initial water content in melt inclusions. Such correlations are mainly reported for samples from island-arc setting (e.g. Roggensack et al., 1997; Cervantes and Wallace, 2003; Wade et al., 2006; Sadofsky et al., 2007) and rather rare for MORB (Saal et al., 2002). The examination of these data sets allows us to constrain the specific conditions of magma crystallization which favor a preservation of initial water content in inclusions. Typical published examples of inclusions, which may have preserved initial water content are observed (1) in island-arc rocks which exhibit clear degassing-driven crystallization trends (crystallization of the host mineral during magma ascent; e.g. Roggensack et al., 1997; Wade et al., 2006; Sadofsky et al., 2007), (2) in rare-olivine phyrlic rocks containing olivines with a narrow interval of compositions in close equilibrium with matrix melt, assumed to be nearly primitive magmas with little fractionation and short residence time in magma chambers (Saal et al., 2002; Kamenetsky et al., 2007), and (3) in hybrid rocks

formed by magma mixing (e.g., Sadofsky et al., 2007). In the latter case, magma mixing could trigger volcanic eruption (Sparks et al., 1977) and thus prevented long storage of hybrid magmas in the crust and re-equilibration of inclusions.

In summary, our experimental results and examination of published data on melt inclusions allow to formulate a general rule for studies aimed at reconstructing magmatic water content from melt inclusions. Only those melt inclusions which interacted with magma having different water content for less than a few hours can be informative of magmatic water content at the moment of inclusion entrapment. This conclusion re-emphasizes the importance of careful studies aimed at estimating the residence time of magmas in the crust (Gaetani and Watson, 2000; Danyushevsky et al., 2002a,b), which are highly important for correct interpretation of melt inclusion data and reconstruction of water content in magmas.

5. Conclusions

We have carried out an experimental study aimed to test the ability of olivine to isolate chemically melt inclusions from host magma on the time scale of few days. The major results of the study are:

- 1) Regardless of the way of water addition to the system (free water or pre-hydrated matrix glass), inclusions in olivine with initially low H₂O contents (~0.5 wt.%) can gain up to ~2.5 wt.% H₂O from the matrix hydrous melt after 2 days of the experimental treatment at 200 MPa pressure and 1140 °C temperature. The concentration of structurally bounded H₂O in olivine increases from less than 10 ppm up to 60 ppm after experiments. Major elements in inclusions maintained equilibria with olivine at hydrous conditions, whereas the concentrations of incompatible elements did not change significantly and remained in strong contrast with the matrix melt.
- 2) An apparent diffusion coefficient of water in our experiments was estimated to be $\geq 5 \times 10^{-12}$ m²/s, indicating that water transport in olivine can be nearly as fast as the proton-vacancy diffusion and at least 3–4 orders of magnitude faster than for other major and trace elements. Proton diffusion cannot explain rapid incorporation of large amounts of water from matrix melt into inclusions. Alternative or additional process, which could be involved, is transport of molecular water through lattice defects and micro-cracks in olivine.
- 3) We suggest that rapid exchange of water between inclusions in olivine and matrix melt or atmosphere is a common natural process, which can explain both anomalously high H₂O content in some trace element depleted inclusions and also dramatic H₂O loss from inclusions in slowly cooled volcanic rocks. Rare cases of good correlation of water and trace elements in suites of co-genetic inclusions imply a very short residence time (a few hours) of the inclusion-bearing olivines in magma with contrasting water content and effective quenching of the inclusions during eruption.

Acknowledgments

We thank D. Christie and K. Hoernle for providing sample from the Galapagos Plateau, M. Thöner and S. Simakin for their help with electron and ion-probe analyses, N. Mironov for help with sample preparation. This work benefited greatly from insightful comments of A. Sobolev, P. Wallace, R. Botcharnikov and three anonymous reviewers on an early version of this manuscript. This research was supported by BMBF (KALMAR project to M.P.) and DFG (Ho 1337/19 to R.A. and F.H.).

Appendix A. Supplementary data

Supplementary data associated with this article can be found, in the online version, at doi:10.1016/j.epsl.2008.05.020.

References

- Almeev, R.R., Holtz, F., Koepke, J., Parat, P., Botcharnikov, R.E., 2007. The effect of H₂O on olivine crystallization in MORB: experimental calibration at 200 MPa. *Am. Mineral.* 92, 670–674.
- Aubaud, C., Hauri, E.H., Hirschmann, M.M., 2004. Hydrogen partition coefficients between nominally anhydrous minerals and basaltic melts. *Geophys. Res. Lett.* 31. doi:10.1029/2004GL021341.
- Bakker, R.J., Jansen, J.B.H., 1994. A mechanism for preferential H₂O leakage from fluid inclusions in quartz, based on TEM observations. *Contrib. Mineral. Petrol.* 116, 7–20.
- Behrens, H., Stuke, A., 2003. Quantification of H₂O contents in silicate glasses using IR spectroscopy—a calibration based on hydrous glasses analyzed by Karl–Fischer titration. *Glass Sci. Technol.* 76, 176–189.
- Bell, D.R., Rossman, G.R., Maldener, J., Endisch, D., Rauch, F., 2003. Hydroxide in olivine: a quantitative determination of the absolute amount and calibration of the IR spectrum. *J. Geophys. Res.* 108 (B2), 2105. doi:10.1029/2001JB000679.
- Berry, A.J., O'Neill, H.S.C., Hermann, J., Scott, D.R., 2007. The infrared signature of water associated with trivalent cations in olivine. *Earth Planet. Sci. Lett.* 261, 134–142.
- Burnham, C.W., 1979. The importance of volatile constituents. In: Yoder, H.S. (Ed.), *The Evolution of the Igneous Rocks*. Princeton University Press, Princeton, NJ, pp. 439–482.
- Cervantes, P., Wallace, P.J., 2003. Role of H₂O in subduction-zone magmatism: new insights from melt inclusions in high-Mg basalts from central Mexico. *Geology* 31, 235–238.
- Chakraborty, S., 1997. Rates and mechanisms of Fe–Mg interdiffusion in olivine at 980–1300 °C. *J. Geophys. Res.* 102, 12,317–12,331.
- Churikova, T., Wörner, G., Mironov, N., Kronz, A., 2007. Volatile (S, Cl and F) and fluid mobile trace element compositions in melt inclusions: implications for variable fluid sources across the Kamchatka arc. *Contrib. Mineral. Petrol.* 154, 217–239.
- Danyushevsky, L.V., Sobolev, A.V., Dmitriev, L.V., 1996. Estimation of the pressure of crystallization and H₂O content of MORB and BABB glasses: calibration of an empirical technique. *Mineral. Petrol.* 57, 185–204.
- Danyushevsky, L.V., Della-Pasqua, F.N., Sokolov, S., 2000. Re-equilibration of melt inclusions trapped by magnesian olivine phenocrysts from subduction-related magmas: petrological implications. *Contrib. Mineral. Petrol.* 138, 68–83.
- Danyushevsky, L., McNeill, A.W., Sobolev, A.V., 2002a. Experimental and petrological studies of melt inclusions in phenocrysts from mantle-derived magmas: an overview of techniques, advantages and complications. *Chem. Geol.* 183, 5–24.
- Danyushevsky, L.V., Sokolov, S., Falloon, T., 2002b. Melt inclusions in phenocrysts: using diffusive re-equilibration to determine the cooling history of a crystal, with implications for the origin of olivine-phyric volcanic rocks. *J. Petrol.* 43, 1651–1671.
- Eiler, J.M., Crawford, A., Elliott, T., Farley, K.A., Valley, J.W., Stolper, E.M., 2000. Oxygen isotope geochemistry of oceanic-arc lavas. *J. Petrol.* 41, 239–256.
- Feig, S.T., Koepke, J., Snow, J.E., 2006. Effect of water on tholeiitic basalt phase equilibria—an experimental study under oxidizing conditions. *Contrib. Mineral. Petrol.* 152, 611–638.
- Ford, C.E., Russel, D.G., Graven, J.A., Fisk, M.R., 1983. Olivine-liquid equilibria: temperature, pressure and composition dependence of the crystal/liquid cation partition coefficients for Mg, Fe²⁺, Ca and Mn. *J. Petrol.* 24, 256–265.
- Gaetani, G.A., Watson, E.B., 2000. Open system behavior of olivine-hosted melt inclusions. *Earth Planet. Sci. Lett.* 183, 27–41.
- Gurenko, A.A., Belousov, A.B., Trumbull, R.B., Sobolev, A.V., 2005. Explosive basaltic volcanism of the Chikurachki Volcano (Kurile arc, Russia): Insights on pre-eruptive magmatic conditions and volatile budget revealed from phenocryst-hosted melt inclusions and groundmass glasses. *J. Volcanol. Geotherm. Res.* 147, 203–232.
- Hauri, E., 2002. SIMS analysis of volatiles in silicate glasses, 2: isotopes and abundances in Hawaiian melt inclusions. *Chem. Geol.* 183, 115–141.
- Hier-Majumder, S., Anderson, I.M., Kohlstedt, D.L., 2005. Influence of protons on Fe–Mg interdiffusion in olivine. *J. Geophys. Res.* 110, B02202. doi:10.1029/2004JB003292.
- Hofmann, A.W., 1997. Mantle geochemistry: the message from oceanic volcanism. *Nature* 385, 219–229.
- Jamtveit, B., Brooker, R., Brooks, K., Larsen, L.M., Pedersen, T., 2001. The water content of olivines from the North Atlantic Volcanic Province. *Earth Planet. Sci. Lett.* 186, 401–415.
- Jarosewich, E.J., Nelen, J.A., Norberg, J.A., 1980. Reference samples for electron microprobe analysis. *Geostand. Newsl.* 4, 43–47.
- Jochum, K.P., et al., 2006. MPI-DING reference glasses for in situ microanalysis: New reference values for element concentrations and isotope ratios. *Geochem. Geophys. Geosyst.* 7. doi:10.1029/2005GC001060.
- Jurewicz, J.G., Watson, E.B., 1988. Cations in olivine, Part 2: Diffusion in olivine xenocrysts, with applications to petrology and mineral physics. *Contrib. Mineral. Petrol.* 99, 186–210.
- Kamenetsky, V.S., Eggins, S.M., Crawford, A.J., Green, D.H., Gasparon, M., Falloon, T.J., 1998. Calcic melt inclusions in primitive olivine at 43°N MAR: evidence for melt-rock reaction/melting involving clinopyroxene-rich lithologies during MORB generation. *Earth Planet. Sci. Lett.* 160, 115–132.
- Kamenetsky, V.S., Pompilio, M., Métrich, N., Sobolev, A.V., Kuzmin, D.V., Thomas, R., 2007. Arrival of extremely volatile-rich high-Mg magmas changes explosivity of Mount Etna. *Geology* 35, 255–258.
- Koga, K., Hauri, E., Hirschmann, M., Bell, D.D., 2003. Hydrogen concentration analyses using SIMS and FTIR: comparison and calibration for nominally anhydrous minerals. *Geochem. Geophys. Geosyst.* 4 (2), 1019. doi:10.1029/2002GC000378.
- Libowitzky, E., Rossman, G.R., 1996. Principles of quantitative absorbance measurements in anisotropic crystals. *Phys. Chem. Miner.* 23, 319–327.
- Mackwell, S.J., Kohlstedt, D.L., 1990. Diffusion of hydrogen in olivine: Implications for water in the mantle. *J. Geophys. Res.* 95 (B4), 5079–5088.
- Massare, D., Métrich, N., Clocchiatti, R., 2002. High-temperature experiments on silicate melt inclusions in olivine at 1 atm: inference on temperatures of homogenization and H₂O concentrations. *Chem. Geol.* 183, 87–98.
- Matveev, S. CHO fluids at upper mantle conditions, Ph.D. thesis, Universität zu Köln, 1997.
- Matveev, S., Stachel, T., 2007. FTIR spectroscopy of OH in olivine: a new tool in kimberlite exploration. *Geochim. Cosmochim. Acta* 71, 5528–5543.
- Métrich, N., Schiano, P., Clocchiatti, R., Maury, R.C., 1999. Transfer of sulfur in subduction settings: an example from Batan Island (Luzon volcanic arc, Philippines). *Earth Planet. Sci. Lett.* 167, 1–14.
- Michael, P., 1995. Regionally distinctive sources of depleted MORB: evidence from trace elements and H₂O. *Earth Planet. Sci. Lett.* 131, 301–320.
- Moretti, R., 2005. Polymerisation, basicity, oxidation state and their role in ionic modelling of silicate melts. *Ann. Geophys.* 48, 583–608.
- Paterson, M.S., 1982. The determination of hydroxyl by infrared absorption in quartz, silicate glasses and similar materials. *Bull. Minéral.* 20–29.
- Petry, C., Chakraborty, S., Palme, H., 2004. Experimental determination of Ni diffusion coefficients in olivine and their dependence on temperature, composition, oxygen fugacity, and crystallographic orientation. *Geochim. Cosmochim. Acta* 68, 4179–4188.
- Portnyagin, M.V., Danyushevsky, L.V., Kamenetsky, V.S., 1997. Coexistence of two distinct mantle sources during formation of ophiolites: a case study of primitive pillow-lavas from the lowest part of the volcanic section of the Troodos Ophiolite, Cyprus. *Contrib. Mineral. Petrol.* 128, 287–301.
- Portnyagin, M.V., Hoernle, K., Plechov, P.Y., Mironov, N.L., Khubunaya, S.A., 2007. Constraints on mantle melting and composition and nature of slab components in volcanic arcs from volatiles (H₂O, S, Cl, F) and trace elements in melt inclusions from the Kamchatka Arc. *Earth Planet. Sci. Lett.* 255, 53–69.
- Qin, Z., Lu, F., Anderson Jr., A.T., 1992. Diffusive re-equilibration of melt and fluid inclusions. *Am. Mineral.* 77, 565–576.
- Rocholl, A.B.E., Simon, K., Jochum, K.P., Molzahn, M., Pernicka, E., Seufert, M., Spettel, B., Stummeier, J., 1997. Chemical characterization of NIST silicate glass certified reference material SRM 610 by ICP-MS, TIMS, LIMS, SSMS, INAA, AAS and PIXE. *Geostandards* 21, 101–114.
- Roedder, E., 1984. *Fluid inclusions*. Miner. Soc. Amer. Book Crafters Inc., Michigan. 644 pp.
- Roggensack, K., Hervig, R.L., McKnight, S.B., Williams, S.N., 1997. Explosive basaltic volcanism from Cerro Negro volcano: Influence of volatiles on eruptive style. *Science* 277, 1639–1642.
- Saal, A.E., Hauri, E.H., Langmuir, C.H., Perfit, M.R., 2002. Vapour undersaturation in primitive mid-ocean-ridge basalt and the volatile content of Earth's upper mantle. *Nature* 419, 451–455.
- Sadofsky, S., Portnyagin, M., Hoernle, K., van den Bogaard, P., 2007. Subduction cycling of volatiles and trace elements through the Central American volcanic arc: evidence from melt inclusions. *Contrib. Mineral. Petrol.* 155, 433–456. doi:10.1007/s00410-007-0251-3.
- Scailliet, B., Pichavant, M., Roux, J., 1995. Experimental crystallization of leucogranite magmas. *J. Petrol.* 36, 663–705.
- Schiano, P., 2003. Primitive mantle magmas recorded as silicate melt inclusions in igneous minerals. *Earth-Sci. Rev.* 63, 121–144.
- Schuessler, J., Botcharnikov, R.E., Behrens, H., Misiti, V., Freda, C., in press. Oxidation state of iron in hydrous phono-tephritic melts. *Am. Mineral.* doi:10.2138/am.2008.2795.
- Sobolev, A.V., 1996. Melt inclusions in minerals as a source of principal petrological information. *Petrology* 4, 209–220.
- Sobolev, A.V., Chaussidon, M., 1996. H₂O concentrations in primary melts from island arcs and mid-ocean ridges: implications for H₂O storage and recycling in the mantle. *Earth Planet. Sci. Lett.* 137, 45–55.
- Sobolev, A.V., Shimizu, N., 1993. Ultra-depleted primary melt included in an olivine from the Mid-Atlantic Ridge. *Nature* 363, 151–154.
- Sobolev, A.V., Sobolev, N.V., Smith, C.B., Dubessy, J., 1989. Fluid and melt compositions in lamproites and kimberlites based on the study of inclusions in olivine. In: Ross, J. (Ed.), 4-th International Kimberlite Conference, GSA Special Publication No.14 Kimberlites and Related Rocks. V.1. Their composition, Occurrence, Origin and Emplacement. Blackwell Sci. Publ., Perth, pp. 220–240.
- Spandler, C., O'Neill, H.S.C., Kamenetsky, V.S., 2007. Survival times of anomalous melt inclusions from element diffusion in olivine and chromite. *Nature* 447, 303–306.
- Sparks, R.S.J., Sigurdsson, H., Wilson, L., 1977. Magma mixing—mechanism for triggering acid explosive eruptions. *Nature* 267, 315–318.
- Stolper, E., Newman, S., 1994. The role of water in the petrogenesis of Mariana Trough magmas. *Earth Planet. Sci. Lett.* 121, 293–325.
- Sun, S.S., McDonough, W.F., 1989. Chemical and isotopic systematics of oceanic basalts: implications for mantle composition and processes. In: Saunders, A.D., Norry, M.J. (Eds.), *Magmatism in the Ocean Basins*, vol. 42. Geological Society Special Publication, London, pp. 313–345.
- Taylor, J.R., Wall, V.J., Pownceby, M.L., 1992. The calibration and application of accurate redox sensors. *Am. Mineral.* 77, 284–295.
- Wade, J.A., Plank, T., Melson, W.G., Soto, G.J., Hauri, E.H., 2006. The volatile content of magmas from Arenal volcano, Costa Rica. *J. Volcanol. Geotherm. Res.* 157, 94–120.
- Wallace, P.J., 2005. Volatiles in subduction zone magmas: concentrations and fluxes based on melt inclusion and volcanic gas data. *J. Volcanol. Geotherm. Res.* 140, 217–240.